

# The influence of current collectors on Tayler instability and electro-vortex flows in liquid metal batteries

N. Weber,<sup>1</sup> V. Galindo,<sup>1</sup> J. Priede,<sup>2</sup> F. Stefani,<sup>1</sup> and T. Weier<sup>1, a)</sup>

<sup>1)</sup>*Helmholtz-Zentrum Dresden - Rossendorf, Bautzner Landstr. 400, 01328 Dresden, Germany*

<sup>2)</sup>*Engineering and Computing, Coventry University, Coventry, CV1 5FB United Kingdom*

The Tayler instability is a kink-type flow instability which occurs when the electrical current through a conducting fluid exceeds a certain critical value. Originally studied in the astrophysical context, the instability was recently shown to be also a limiting factor for the upward scalability of liquid metal batteries. In this paper, we continue our efforts to simulate this instability for liquid metals within the framework of an integro-differential equation approach. The original solver is enhanced by multi-domain support with Dirichlet-Neumann partitioning for the static boundaries. Particular focus is laid on the detailed influence of the axial electrical boundary conditions on the characteristic features of the Tayler instability, and, secondly, on the occurrence of electro-vortex flows and their relevance for liquid metal batteries.

PACS numbers: 47.11.Df 47.20.-k 52.30.Cv

Keywords: liquid metal battery, simulation, OpenFOAM, electro vortex flow, Tayler instability

---

<sup>a)</sup>Electronic mail: t.weier@hzdr.de

## I. INTRODUCTION

It is well known that the interaction of an electrical current with its own magnetic field in a conducting fluid can create equilibrium states that are not always stable. For example, the electrical discharge in a plasma column can be prone either to the axisymmetric “sausage” or the non-axisymmetric “kink” instability. At the conductivity and viscosity values typical for plasmas, such instabilities are common, and special care must be taken to avoid them. For the case of a  $z$ -pinch, and similarly for Tokamak geometry, this is expressed by the Kruskal-Shafranov condition stating that the kink instability can only be suppressed by applying an additional longitudinal magnetic field<sup>1</sup>. Things are different for liquid metals, in which the high values of resistivity and viscosity play a stabilizing role. For the paradigmatic case of a homogeneous current through a cylindrical liquid metal column, this type of instability is governed by the ratio of magnetic to viscous forces, expressed by the square of the Hartmann number

$$\text{Ha} = B_0 R (\sigma / \rho \nu)^{1/2},$$

where  $B_0 = B_\varphi(R)$  is the azimuthal magnetic field at the cylinder radius  $R$ ;  $\sigma$ ,  $\rho$ , and  $\nu$  are the conductivity, density and kinematic viscosity of the fluid. Beyond a critical value of  $\text{Ha} \simeq 20$ , see Rüdiger et al.<sup>2</sup>, a non-axisymmetric flow pattern will appear in the fluid reaching a mean velocity value  $V$  whose corresponding Reynolds number  $\text{Re} = RV/\nu$  scales as  $\text{Re} \sim \text{Ha}^2$ .

In contrast to the vast experience with the kink-type instability in plasma physics, its occurrence in a liquid metal was experimentally demonstrated only recently<sup>3</sup>. This instability, which needs a certain critical current to overcome the stabilizing effect of resistivity and viscosity, is referred to as the *Taylor instability* (TI) – the term originally restricted to the destabilizing effect of a magnetic field on a stably stratified fluid in cosmic bodies. In this astrophysical context, the TI had been discussed in connection with a non-linear stellar dynamo mechanism<sup>4</sup>, and the fast slow-down of white dwarfs<sup>5</sup>.

Apart from its astrophysical significance, the TI may also be relevant for the applied problem connected with the revived interest in liquid metal batteries (LMB), which are promising as a relatively cheap storage for the highly fluctuating renewable energies<sup>6</sup>. Liquid metal batteries consist basically of a self-assembling stratified system of a heavy liquid metal or metalloid (e.g., Bi, Sb) at the bottom, a molten salt mixture as electrolyte in the middle,

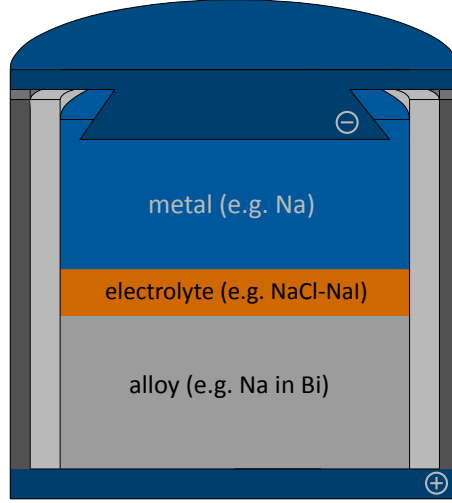


FIG. 1. Sketch of a typical Liquid Metal Battery (LMB).

and a light alkaline or earth alkaline metal (e.g., Na, Mg) at the top (see Fig. 1). Choosing Na and Bi as an example, Na will lose one electron during the discharge process, turning into  $\text{Na}^+$ . This ion diffuses through the electrolyte into the lower Bi layer where it is reduced and alloys with Bi to NaBi.

To be economically competitive, such batteries should be built rather large. With envisioned current densities of up to  $10 \text{ kA/m}^2$ , a base area of  $\approx 1 \text{ m}^2$  would immediately lead to total currents of several kA, which poses a certain risk of the TI. The TI-driven flow would then endanger the integrity of the (poorly conducting) electrolyte layer<sup>7</sup>, which should usually be chosen as thin as possible in order to reduce energy losses due to Joule heating. Despite the fact that it is well possible to suppress the TI by either using a back-directed current in the centre<sup>8</sup>, or by invoking the Kruskal-Shafranov idea, i.e. by applying an additional axial magnetic field<sup>7</sup>, a more detailed knowledge of the characteristics of the TI in liquid metal batteries is still desirable.

Although strong fluid flows represent a danger for the LMB, a slight flow in the cathode compartment may be advantageous. Several researchers observed concentration polarisation<sup>6,9-12</sup> caused by mass transfer limitations while (dis-)charging LMBs. These may be due to, for example, a concentration of reaction products at the electrolyte-alloy interface. Here, a careful mixing of the alloy would be favourable<sup>11,12</sup>, e.g. by exploiting electro-vortex flow or thermal convection<sup>13</sup>.

In a recent paper<sup>14</sup>, we made a first attempt to simulate the TI for realistic material

parameters of liquid metals. Rather than applying the usual method of solving the coupled system of Navier-Stokes equation for the velocity and induction equation for the magnetic field, we utilized an integro-differential equation approach in which the hydrodynamics is still simulated by the Navier-Stokes equation while the electromagnetic part is solved by applying a Poisson equation for the electric potential and the Biot-Savart law for the magnetic field. With this method we were able to confirm the experimental results of Seilmayer et al.<sup>3</sup>, and to predict the critical currents for onset of the TI for varying aspect ratio.

In this first approach we assumed the initial current distribution to be strictly vertical and the magnetic field to depend spatially only on the radius. Also the axial electrical boundary conditions at the current collectors were simplified by setting the electric potential to a constant on the whole interface, which corresponds to perfectly conducting solid current collectors. Using this approach we determined only the current perturbation in the liquid but ignored the currents closing through the well conducting collectors. Application of Biot-Savart law to open current loops resulted in not entirely correct distribution of the magnetic field perturbation.

In the present paper, we aim at clarifying the previously neglected effect of the current distribution in the current collectors on the characteristics of the TI. First, we extend the numerical scheme of Weber et al.<sup>14</sup> by including iterative solution of the Laplace equation for the electric potential in the solid current collectors. In a second step, we focus on the initial current and magnetic field distribution. We solve a Laplace equation for the electric potential in the whole domain in order to obtain the initial current distribution. Compared to the simplified approach of Weber et al.<sup>14</sup>, we observe now also radial currents, driving an additional electro-vortex flow.

As a main result we show that an appropriate design of current collectors is very important in regard to the resulting electro vortex flow. The effect of missing current collectors on the TI is often considerable, but in certain cases it will be justified to restrict the attention to the numerics in the liquid. The developed method is a first step towards a detailed investigation of the coupled problem of TI, electro-vortex flow, thermal convection and interfacial instabilities at the boundaries between the three layers of a liquid metal battery.

## II. MATHEMATICAL MODEL

In this section, we will basically reiterate the derivation of the integro-differential equation approach as it was developed by Weber et al.<sup>14</sup> for the numerical simulation of the TI, but will enhance it with a description of the treatment of the electric potential in the solid current collectors.

The fluid dynamics in a liquid metal is governed by the Navier-Stokes equation (NSE) for the velocity  $\mathbf{v}$ ,

$$\partial_t \mathbf{v} + (\mathbf{v} \cdot \nabla) \mathbf{v} = -\frac{1}{\rho} \nabla p + \nu \Delta \mathbf{v} + \frac{1}{\rho} \mathbf{f}, \quad (1)$$

where  $p$  denotes the pressure,  $\rho$  the density,  $\nu$  the kinematic viscosity, and  $\mathbf{f}$  the body force density. Further, the continuity equation  $\nabla \cdot \mathbf{v} = 0$  is needed to ensure the incompressibility of the fluid.

Consider now an electrical current density  $\mathbf{J}$  in the fluid, together with the magnetic field  $\mathbf{B}$  related to it via  $\mu_0 \mathbf{J} = \nabla \times \mathbf{B}$ , with  $\mu_0$  being the permeability of the free space (magnetic materials are not treated in this paper). The cross product of  $\mathbf{J}$  and  $\mathbf{B}$  gives the Lorentz force, which is the only body force to be considered in the following:

$$\mathbf{f} = \mathbf{f}_L = \mathbf{J} \times \mathbf{B}. \quad (2)$$

The total magnetic field  $\mathbf{B}$  consists of two parts: the static field  $\mathbf{B}_0$ , generated by the externally applied current  $I$  (or the corresponding current density  $\mathbf{J}_0$ ), and the induced magnetic field  $\mathbf{b}$ , generated by the flow induced current  $\mathbf{j}$ . It is essential to note that in our problem  $\mathbf{b}$  must not be neglected in the expression for the Lorentz force since its product with the applied current  $\mathbf{J}_0$  is of the same order as the product of  $\mathbf{B}_0$  with the induced current  $\mathbf{j}$ .

A rigorous way to compute the magnetic field evolution is by solving the induction equation

$$\partial_t \mathbf{B} + (\mathbf{v} \cdot \nabla) \mathbf{B} = (\mathbf{B} \cdot \nabla) \mathbf{v} + \frac{1}{\mu_0 \sigma} \Delta \mathbf{B}. \quad (3)$$

The solution of this equation requires suitable boundary conditions for the magnetic field, which can be implemented either by solving a Laplace equation in the exterior of the fluid<sup>15,16</sup>, or by equivalent boundary element methods<sup>17–19</sup>.

In the following, we adopt a method proposed by Meir et al.<sup>20</sup> for the quasi-stationary

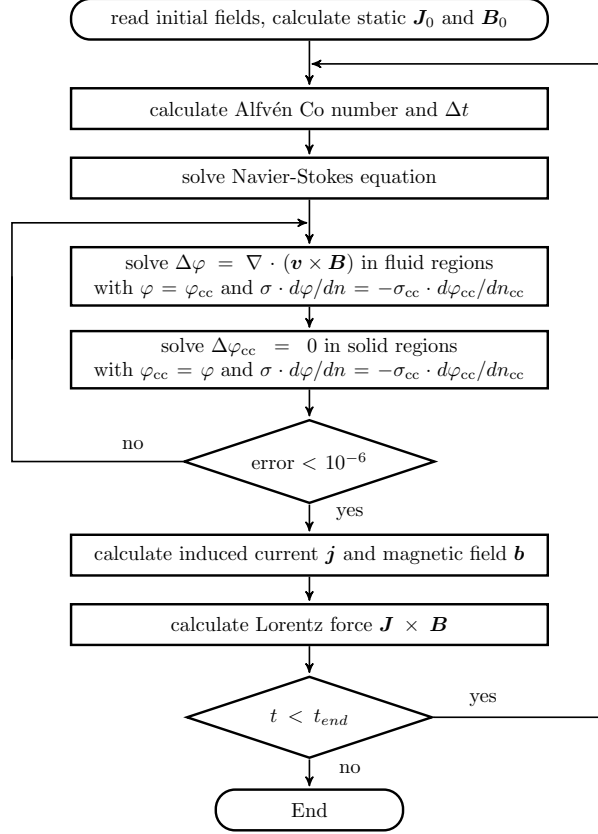


FIG. 2. Flow chart of the simulation model.

case, i.e. we compute the magnetic field using the Biot-Savart law

$$\mathbf{b}(\mathbf{r}) = \frac{\mu_0}{4\pi} \int dV' \frac{\mathbf{j}(\mathbf{r}') \times (\mathbf{r} - \mathbf{r}')}{|\mathbf{r} - \mathbf{r}'|^3}, \quad (4)$$

which is the inversion of Ampère's law  $\nabla \times \mathbf{b} = \mu_0 \mathbf{j}$ . Therefore, the problem is shifted from the determination of the magnetic field  $\mathbf{b}$  to the determination of the current density  $\mathbf{j}$ .

The flow chart of the numerical algorithm (Fig. 2) is similar to that worked out by Weber et al.<sup>14</sup>, with the exception that we need an additional loop to match the solution for the electric potential in the current collectors to that in the liquid metal. Assuming the current  $I$  through our cylindrical vessel as given (e.g., the battery charging current), we compute the corresponding current density  $\mathbf{J}_0$ , and the associated static magnetic field  $\mathbf{B}_0$ . In a first step, we assume the current density to be constant in the whole domain and the magnetic field as resulting from an infinite long cylinder. This allows us to study the influence of the current collectors on the induced currents only. Thereafter, we also consider the feeding lines of the battery by imposing a constant electric potential on the interface between current collector and feeding line and solving a Laplace equation in the solid and liquid domains.

The static magnetic field  $\mathbf{B}_0$  is computed by using the Biot-Savart law. The field of the (infinitely long) feeding lines is added. For that case, the modified current distribution has radial components, as well, and the magnetic field slightly declines close to the current collectors. Previously, the static Lorentz Force  $\mathbf{J}_0 \times \mathbf{B}_0$  had only radial components – now axial components appear, driving electro-vortex flows in the vicinity of the current collectors.

In the main loop of our numerical scheme, the Navier-Stokes equation (1) is solved first, followed by a velocity corrector step to ensure continuity ( $\nabla \cdot \mathbf{v} = 0$ ). Then we have to find the electric current density, both in the liquid metal where  $\mathbf{v} \neq 0$ , and in the solid current collectors where  $\mathbf{v} = 0$ . Assuming the magnetic Reynolds number  $Rm = \mu_0 \sigma R v$  on the basis of the TI-triggered velocity scale  $v$  to be small, we can invoke the quasistatic approximation<sup>21</sup>. This means that we express the electric field by the gradient of an electrostatic potential,  $\mathbf{E} = -\nabla\Phi$ . Applying the divergence operator to Ohm's law in moving conductors,  $\mathbf{j} = \sigma(-\nabla\Phi + \mathbf{v} \times \mathbf{B})$ , and demanding charge conservation,  $\nabla \cdot \mathbf{j} = 0$ , we arrive at the Poisson equation

$$\Delta\varphi = \nabla \cdot (\mathbf{v} \times \mathbf{B}) \quad (5)$$

for the perturbed electric potential  $\varphi = \Phi - \Phi_0$ , where  $\Phi_0$  is the potential according to the externally applied current. Since no current can flow through the insulating rim of the cylindrical vessel, we assume here  $\mathbf{n} \cdot \nabla\varphi = 0$ , where  $\mathbf{n}$  is the surface normal vector.

The new point compared to Weber et al.<sup>14</sup> is now that we have to consider two regions with different conductivities. In the liquid metal, with conductivity  $\sigma$ , we have to solve the Poisson equation with  $\nabla \cdot (\mathbf{v} \times \mathbf{B})$  as the source term. In the solid current collector region, with conductivity  $\sigma_{cc}$ , this source term is absent, and we have to solve the Laplace equation  $\Delta\varphi_{cc} = 0$ . What is still needed are the continuity conditions for the potential and the normal current component at the interface between the two regions. The fastest convergence for this Dirichlet-Neumann partitioning is obtained by combining the two boundary condition to a single Dirichlet condition for the interface potential

$$\varphi_i = \frac{\varphi_{cc}\sigma_{cc}/\delta_{cc} + \varphi\sigma/\delta}{\sigma_{cc}/\delta_{cc} + \sigma/\delta} \quad (6)$$

with  $\varphi_{cc}$  and  $\varphi$  denoting the potential in the cell centres next to the boundary and  $\delta_{cc}$  and  $\delta$  the distance between cell centre and boundary. The subscript  $cc$  stands here for the solid current collector, whereas the variables without subscripts refer to the liquid metal

region. The convergence criterion is  $10^{-6}$ , where the better conducting region is taken for determining the relative error.

Having derived the potential in the fluid by solving the Poisson equation, we easily recover the current density induced by the fluid motion as

$$\mathbf{j} = \sigma (-\nabla\varphi + \mathbf{v} \times \mathbf{B}) \quad (7)$$

and then the induced magnetic field by using the Biot-Savart law (4). As an improvement to Weber et al.<sup>14</sup>, we include now also the current distribution in the current collectors. The total current density is

$$\mathbf{J} = \mathbf{J}_0 + \mathbf{j}. \quad (8)$$

In a last step, the Lorentz force, to be implemented into the Navier-Stokes equation, is calculated according to

$$\mathbf{f}_L = (\sigma (-\nabla\varphi + \mathbf{v} \times (\mathbf{B}_0 + \mathbf{b})) + \mathbf{J}_0) \times (\mathbf{B}_0 + \mathbf{b}). \quad (9)$$

It should be noticed again that the (small) induced magnetic field  $\mathbf{b}$  cannot be omitted here, since its product with the (large) imposed current  $\mathbf{J}_0$  is of the same order as the product of the (small) induced current  $\mathbf{j}$  with the (large) magnetic field  $\mathbf{B}_0$ .

### III. EXPLORING THE ROLE OF CURRENT COLLECTORS

In this section we will study in detail the effect of the current distribution in the solid current collectors on the TI. We chose a liquid metal column of constant height  $H = 1.2$  m, diameter  $D = 2R = 1$  m, aspect ratio  $H/D = 1.2$  and electric conductivity  $\sigma$ . We apply an electrical current corresponding to  $\text{Ha} = 250$  and vary the height  $H_{cc}$  as well as the conductivity  $\sigma_{cc}$  of the solid current collectors. Remember that the latter ones were not included by Weber et al.<sup>14</sup> where the simplified condition  $\varphi = \text{const}$  was chosen as interface condition at top and bottom of the liquid metal column, and the currents in the current collectors were also ignored in the Biot-Savart law. From physical arguments, we anticipate that in long liquid metal columns the effect of the detailed current distribution at the ends of the current collectors should be negligible, but that it might still be significant in shallow layers.



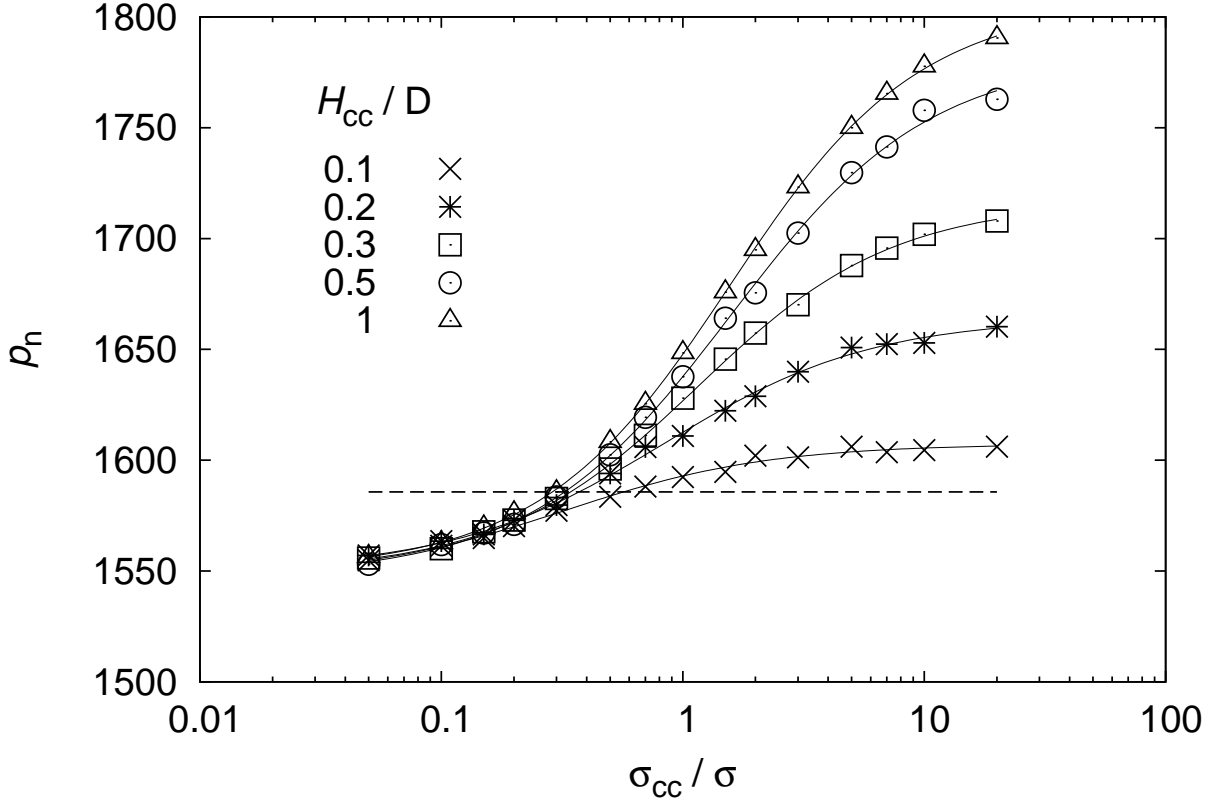


FIG. 3. The growth rate of the TI against the conductivity ratio of current collectors of various height for a cylindrical liquid metal column with aspect ratio  $H/D = 1.2$ , diameter  $D = 1$  m and  $Ha = 250$ . The physical growth rate is normalised by the inverse of the viscous time scale  $R^2/\nu$ . The dashed line is the growth rate for a simulation with the equipotential boundary conditions and ignored current perturbation in the collectors.

We expect the current collectors to influence the magnitude of the fluid flow as well as the growth rate of the TI. Figure 3 shows the latter for current collectors of various height and an electric conductivity of 0.05 up to 20 times of the liquid metal. The height of the current collector varies from 10 to 100 % of the diameter.

The resulting curves are fitted well by an arctangent function with the constants depending on conductivity and aspect ratio of the current collector. Choosing a poorly conducting current collector, the growth rate approaches an asymptotic minimum (Fig. 3, left). This is the same value for all current collectors, regardless of their aspect ratio. We will show later, that current collectors of low conductivity force the current loops to close already within the

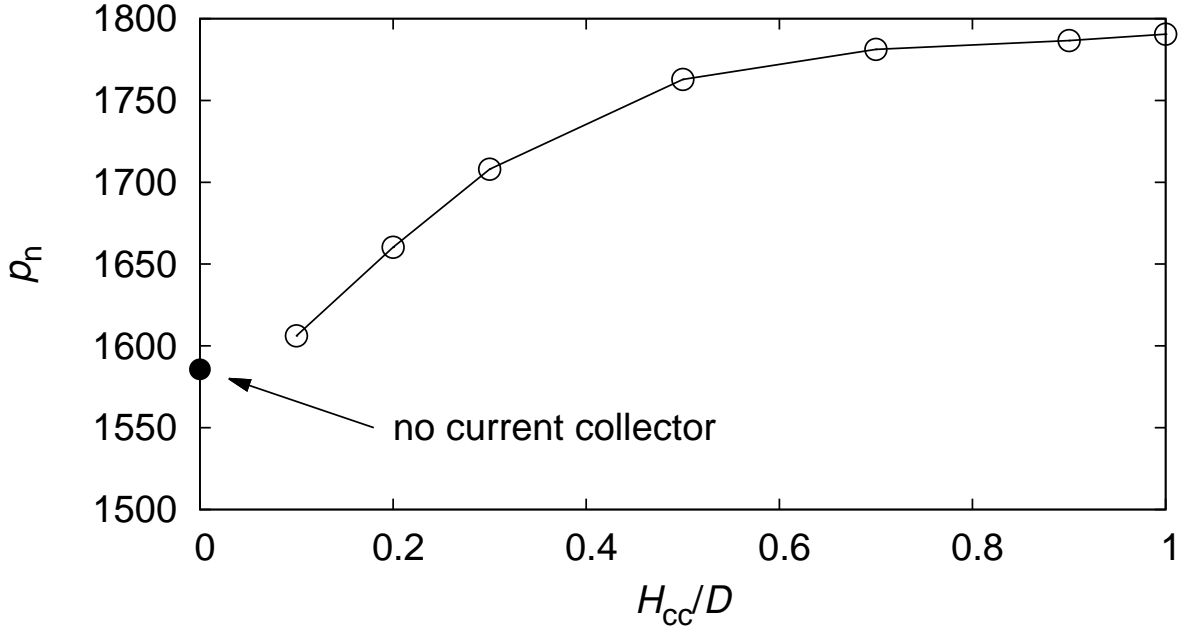


FIG. 4. The growth rate of the TI normalised by the inverse of the viscous time scale  $R^2/\nu$  against the height of current collector for a cylindrical liquid metal column with aspect ratio  $H/D = 1.2$ , diameter  $D = 1$  m, the applied current corresponding to  $Ha = 250$ , and the conductivity ratio of solid and liquid regions  $\sigma_{cc}/\sigma = 20$ .

liquid metal. Very little current perturbation spreading into the poorly conducting current collector makes the instability insensitive to the height of the collector.

Turning to the current collectors of a high relative conductivity compared to the liquid metal (Fig. 3, right) we observe that the growth rate tends to an asymptotic maximum as the height of the current collector becomes comparable to the diameter of the cylinder. Obviously, this is a typical vertical distance over which the currents close in the solid current conductors. The magnetic field of these currents slightly increases the growth rate of the TI. In Fig. 4 we show again the growth rate of the TI, but for a fixed conductivity ratio of  $\sigma_{cc}/\sigma = 20$ , i.e. for very well conducting current collectors. With increasing the height, the growth rate increases, too, approaching an asymptotic maximum. A well conducting current collector which is as high as wide allows almost all currents to close. Further increase of the collector height has almost no effect on the TI.

Another important aspect is the comparison to the growth rate of the (old) simulation

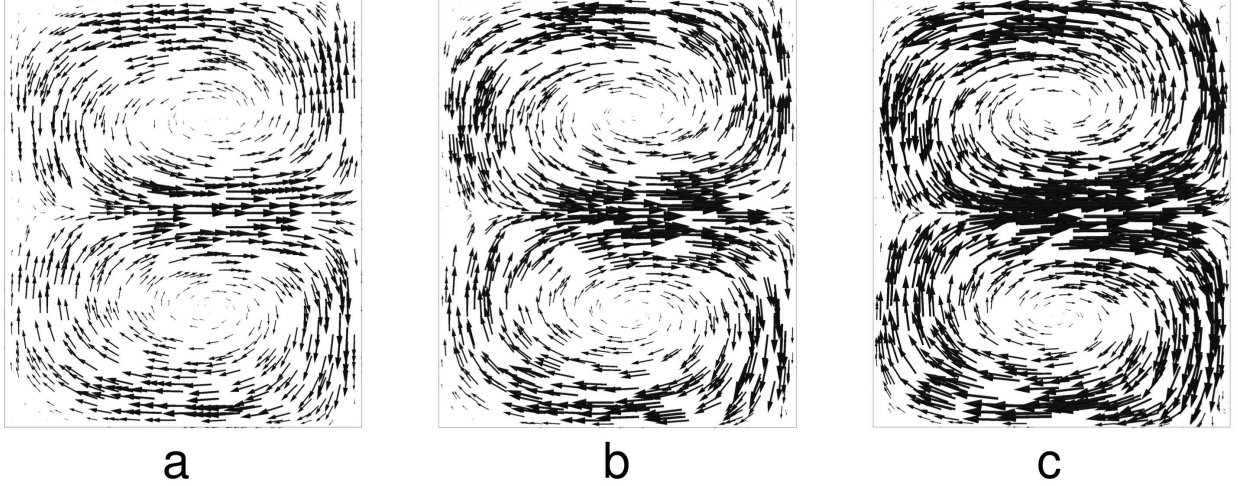


FIG. 5. Velocity field of a saturated TI in a cylinder with  $D = 1$  m,  $H = 1.2$  m and  $Ha = 250$  without current collector (a) and current collectors with aspect ratio  $H_{cc}/D$  of 0.1 (b) and 0.5 (c) and constant conductivity ratio  $\sigma_{cc}/\sigma = 5$ .

without current collectors (Fig. 3, dotted line and Fig. 4, black dot). As we will show later, omitting the current collectors has no grave effect on the current perturbation in the liquid metal. The TI is affected by the current perturbation penetrating into the well conducting current collectors which was ignored in the previous simulation. The effect of this omission is illustrated by the asymptotic value for an infinitely flat current collector (aspect ratio  $H_{cc}/D = 0$ ) shown in Fig. 4.

We will now discuss some exemplary cases in order to illustrate our preceding argumentation. First of all, we will explore the effect of the aspect ratio of the current collectors for the conductivity ratio  $\sigma_{cc}/\sigma = 5$ . Three cases are considered: without current collector (a), with a flat current collector (b) and a high one (c) (see Figs. 5,6 and 7). In the following, we will focus on the saturated TI and ignore the considerably different flow fields which may sometimes be observed during the exponential growth phase of the TI due to spontaneous symmetry breaking<sup>22</sup>.

Figure 5 illustrates the velocity field for the three paradigmatic cases. We observe clearly a globally increasing velocity when adding a current collector (b) and rising its height (c). Interestingly, the form of the convection cells does not change. Comparing Figs. 6a and c, an increase of the induced current of approximately 50% can be observed when adding a current collector of aspect ratio  $H_{cc}/D = 0.5$ . Again, there is no obvious qualitative

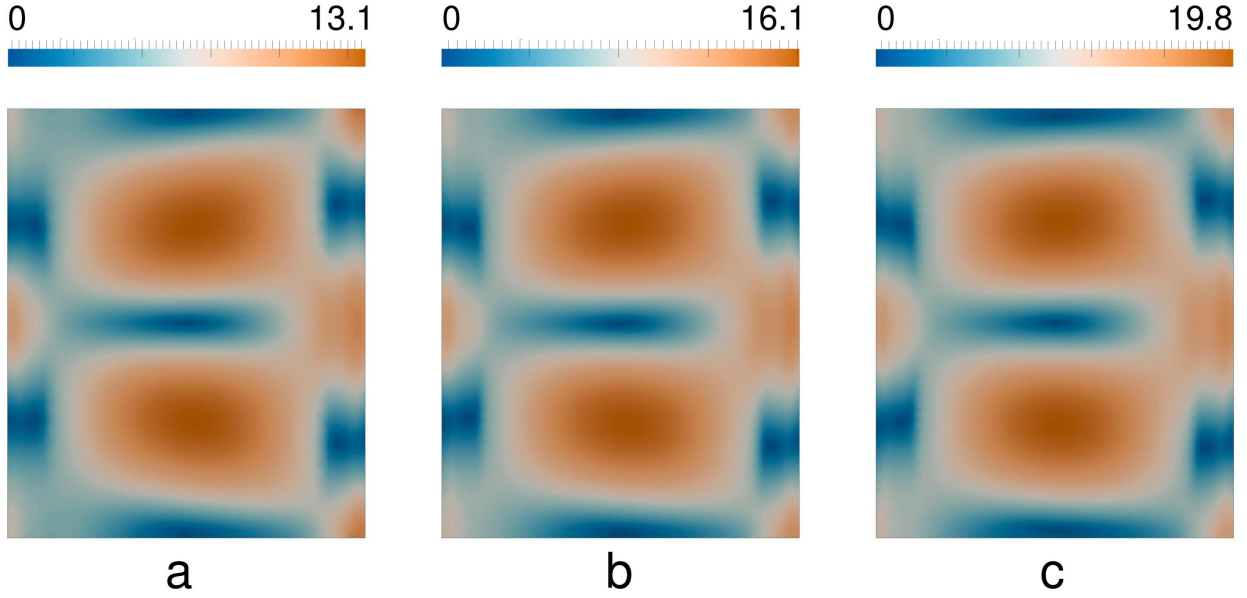


FIG. 6. Magnitude of the induced current density in  $\text{A/m}^2$  of the saturated TI in a cylinder with  $D = 1 \text{ m}$ ,  $H = 1.2 \text{ m}$  and  $\text{Ha} = 250$  without current collector (a) or a current collector of aspect ratio  $H_{cc}/D$  of 0.1 (b) and 0.5 (c). The conductivity ratio between solid and liquid region is  $\sigma_{cc}/\sigma = 5$ .

difference between the simulation with (b,c) and without (a) current collector. In Fig. 7 we show now the current lines in the liquid metal column and the current collectors as well, using the same geometry as before. Omitting the current collectors (Fig. 7a), we can clearly see that the current lines do not close, while they do partially so for flat current collectors (Fig. 7b) and even better for high ones (Fig. 7c). Note also that the disturbed potential at the interfaces is not constant as assumed previously<sup>14</sup> and its nonuniformity increases considerably with increasing current collectors aspect ratio (Fig. 7b and c).

Having explored the role of the current collectors height, we will focus now on its electric conductivity. We compare three current collectors of fixed height  $H_{cc}/D = 0.5$  (see Fig. 8). First, we consider a very poorly conducting solid current collector with a conductivity of  $1/20$  of the liquid metal (Fig. 8a). It is remarkable, that almost all currents close within the liquid metal, with a concentration at the top and bottom of the cylinder. When the conductivity of the current collector is increased to the same value as of the liquid metal, there are much less currents closing near the interface (Fig. 8b). A further elevation of conductivity amplifies this effect (Fig. 8c). At the same time, the maximum value of induced currents almost doubles. While poorly conducting current collectors make the induced current lines close

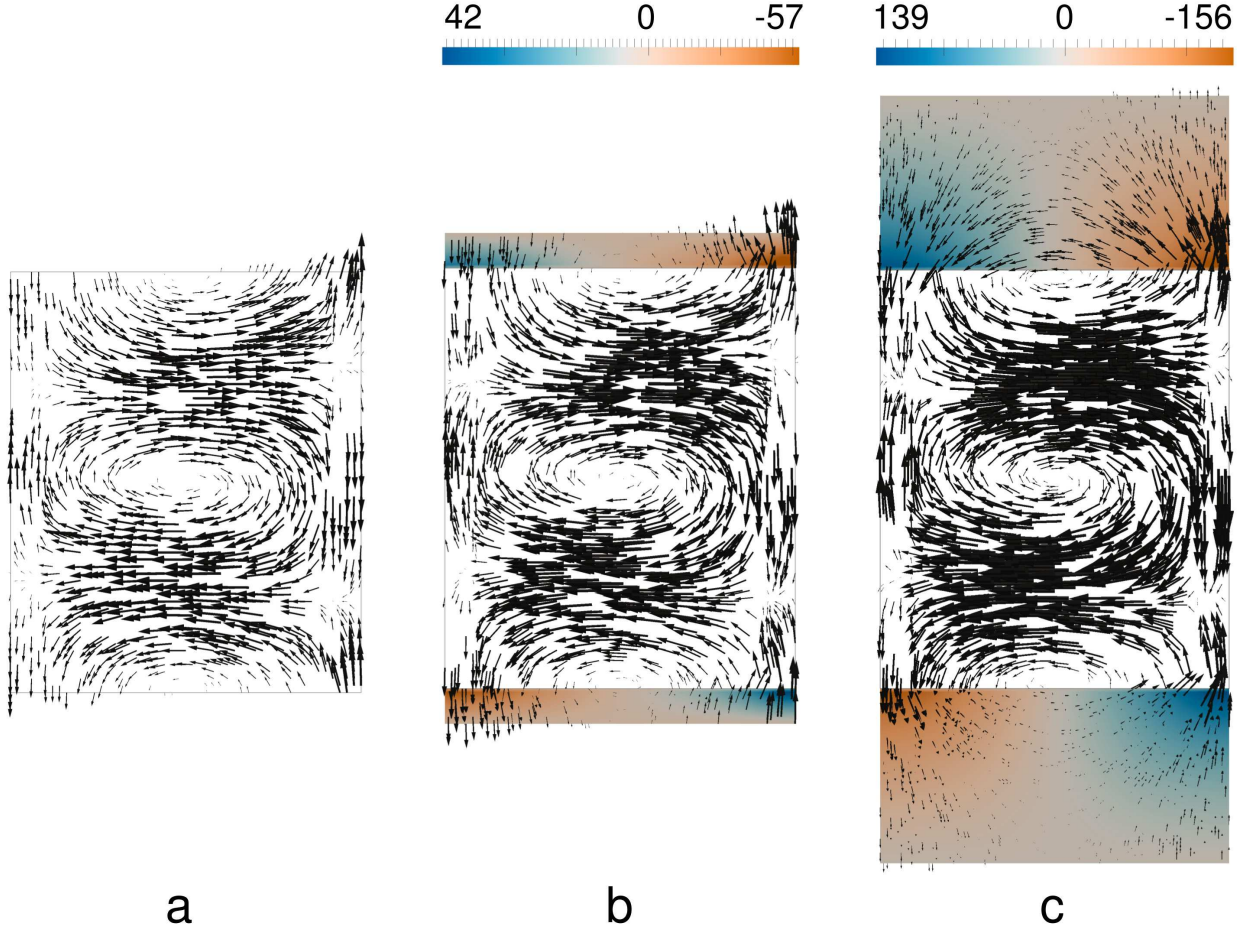


FIG. 7. Electric potential perturbation (nV) in the current collectors and the induced current lines in the saturated TI. The geometry consists of a cylindrical liquid metal column with  $D = 1$  m,  $H = 1.2$  m without (a) or with a current collector of aspect ratio  $H_{cc}/D = 0.1$  (b) and  $0.5$  (c). For the last two cases the current collectors are five times better conducting than the fluid ( $\sigma_{cc}/\sigma = 5$ .)

within the liquid metal (Fig. 8a), the equipotential boundary conditions, which effectively model perfectly conducting collectors, result in the induced current lines running in and out of the liquid metal through the top and bottom interfaces (see Fig. 7a).

Knowing the influence of current collectors on liquid metal columns of aspect ratio  $H/D = 1.2$ , one may expect the effect to be much stronger on very flat cells. On the other hand, the current collectors may be neglected for tall liquid metal columns, as the influence should be limited to the top and bottom regions with length comparable to the diameter of the cylinder. In order to confirm this, we plot the critical Hartmann number for onset of the TI for a liquid metal column of different height (Fig. 9). The diameter of



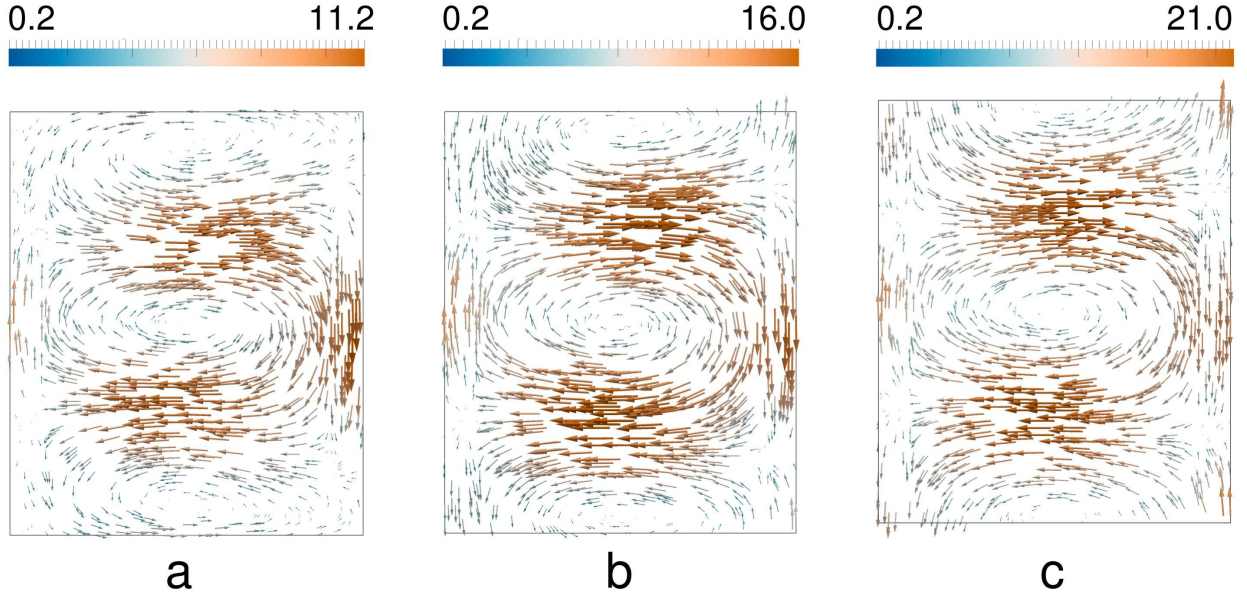


FIG. 8. Induced current density in  $\text{A/m}^2$  of the saturated TI in a cylindrical liquid metal column ( $D = 1 \text{ m}$ ,  $H = 1.2 \text{ m}$ ) with a current collector of constant height  $H_{cc} = 0.5 \text{ m}$  and an applied current corresponding to  $\text{Ha} = 250$ . The conductivity ratio of solid to liquid region  $\sigma_{cc}/\sigma$  is  $1/20$  (a),  $1$  (b) and  $20$  (c). The colour indicates the modulus of the current density.

the column ( $D = 1 \text{ m}$ ) and the current collectors aspect ratio  $H_{cc}/D = 0.1; 0.3$  is constant. At this point it should be noted that the number of convection cells depends markedly on (very) small changes of the column height, see also Weber et al.<sup>14</sup>. The current collector will surely influence the number of vortices, as well, and may thus induce irregularities, like plateaus, in the plot.

Comparing the new simulation for a cylindrical liquid metal column (Fig. 9, black line) to previous simulation for cubic geometries<sup>14</sup>, there are no plateaus of the critical current any more. We assume these plateaus to be caused by the interaction of the cubic geometry and the transition between different numbers of convection cells. Returning to Fig. 9 we observe an almost identical critical current for onset of the TI for very high liquid metal columns, regardless of the current collectors. Interestingly, very flat current collectors ( $\circ$ ) slightly increase the critical current, when flattening the liquid metal column. Although this effect is not very distinct, it is not what we expect (see also Fig. 3). Higher current collectors ( $\Delta$ ) show a very nonuniform variation: for flat liquid metal columns they decrease the critical current while increasing it clearly for an aspect ratio  $H/D$  between  $0.5$  and  $1.5$ . We suspect

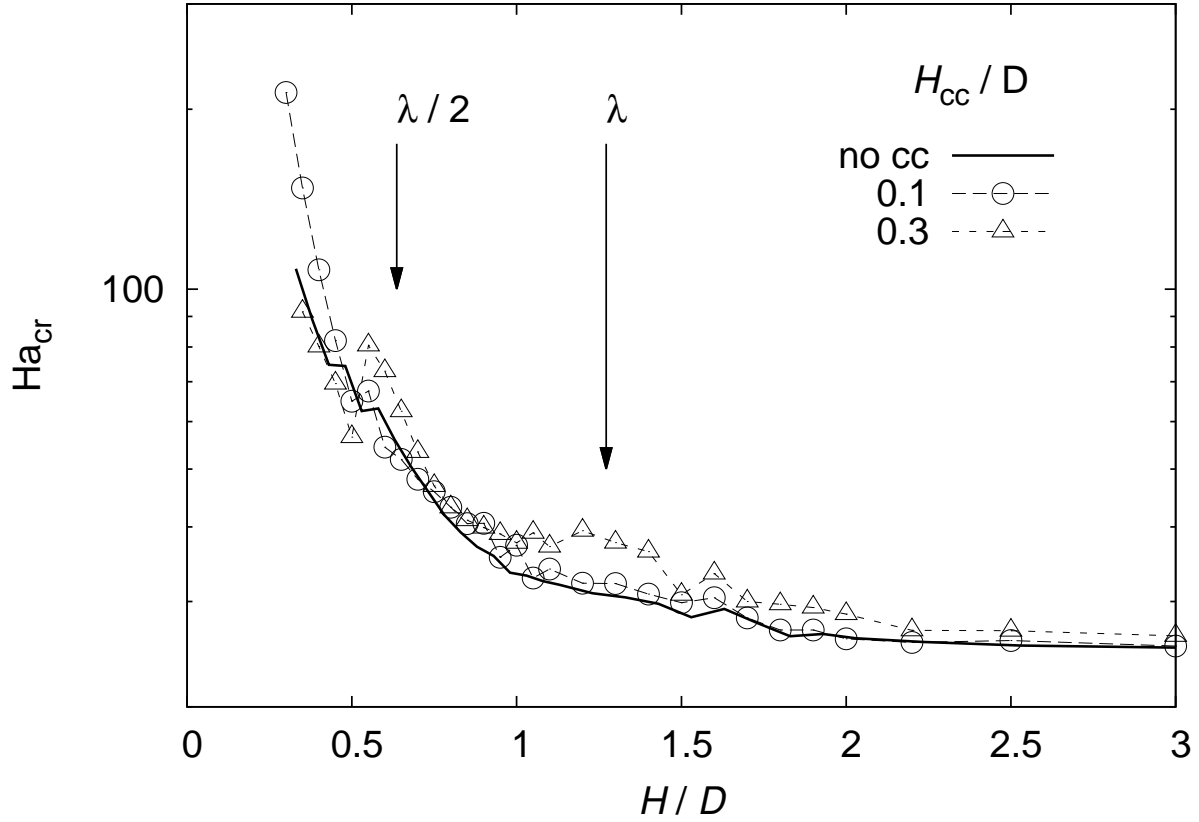


FIG. 9. Critical Hartmann number for onset of the TI depending on the aspect ratio of the liquid metal column. The current collectors have twice the conductivity of the fluid ( $\sigma_{cc}/\sigma = 2$ ), the diameter is  $D = 1$  m.

this behaviour to be caused by the transition between different numbers of TI vortices in relation to the current collectors. However, a detailed explanation has to be postponed.

#### IV. EXPLORING THE ROLE OF THE FEEDING LINES

In the preceding section we considered the induced current closing in the current collector and investigated its influence on the growth rate of the TI. Now, we add the feeding line above of the upper, and below of the lower current collector. The diameter of the wires is assumed to be half of that of the current collectors (see the grey surface in Fig. 10a). In the following we will consider how electrically driven vortex flows arise and how to simulate them. After describing interaction of these flows with the TI we will shortly describe how they scale with the Hartmann number, the current collectors aspect ratio and its electric

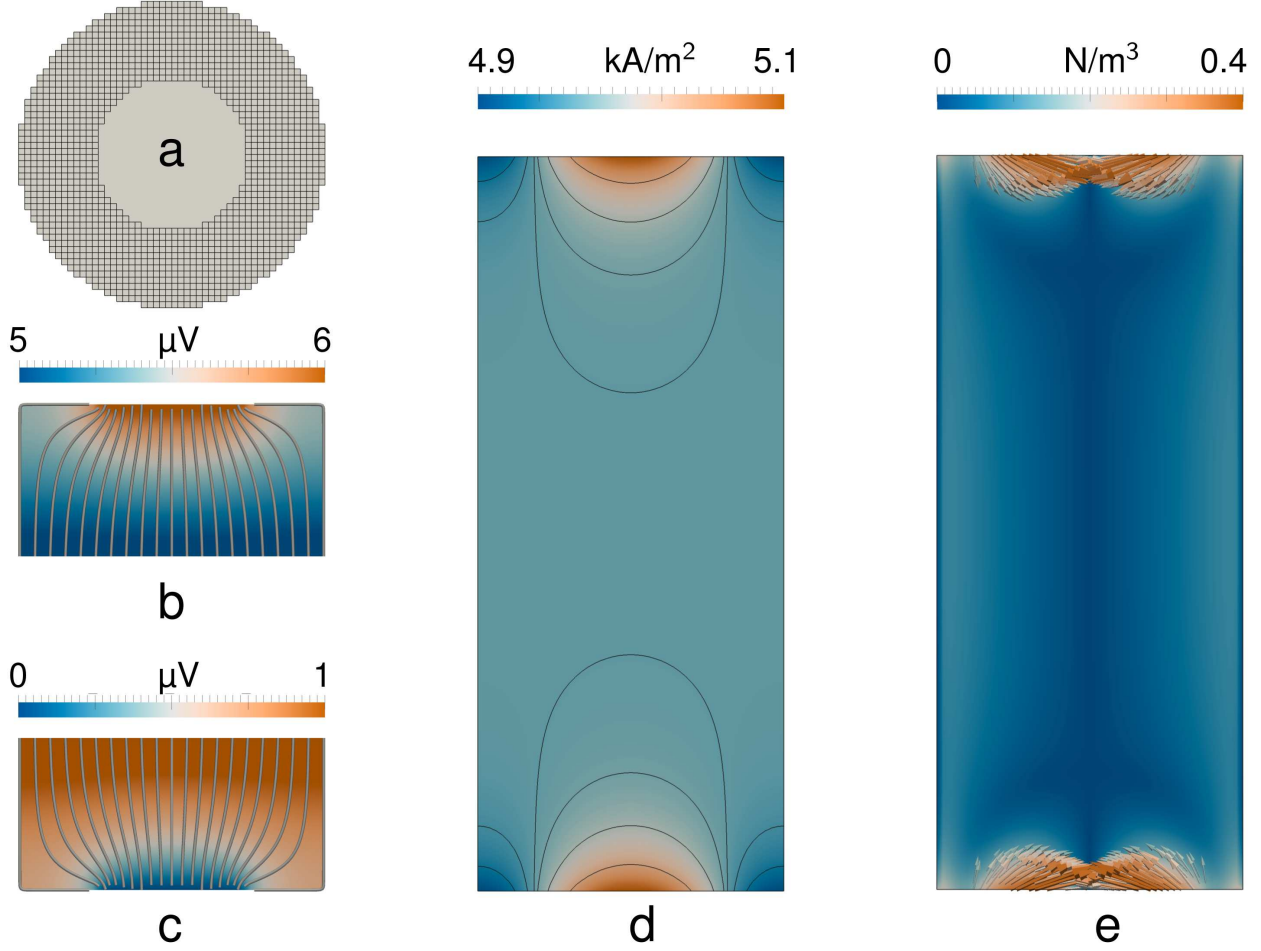


FIG. 10. The top view of the current collector with the boundary condition  $\varphi = 0$  being applied on a circular area with the diameter  $d = D/2 = 0.5\text{ m}$  at the height  $H_{cc} = 0.5\text{ m}$  (a); the current paths and the potential in the upper (b) and lower (c) current collector; the current distribution in the liquid metal (d) and the “disturbed” Lorentz force (e) calculated by subtracting the Lorentz force for the infinite cylinder in order to visualise the origin of the electro-vortex flow. Here the current collectors have the same conductivity as the liquid metal column (of height  $H = 2.4\text{ m}$ ) and the applied current corresponds to  $\text{Ha} = 100$ .

conductivity.

In the previous section, the initial potential  $P_0$  was determined by setting  $P_0 = \text{const}$  on the entire surface of the current collector. Now, we use this boundary condition only on the interface between the feeding line and the current collector (see the grey area in Fig. 10a). Thus, the static potential  $P_0$  is not longer radially uniform (see Figs. 10b and c). This affects the base current density  $\mathbf{J}_0$ , which in our previous model was purely vertical. Now,



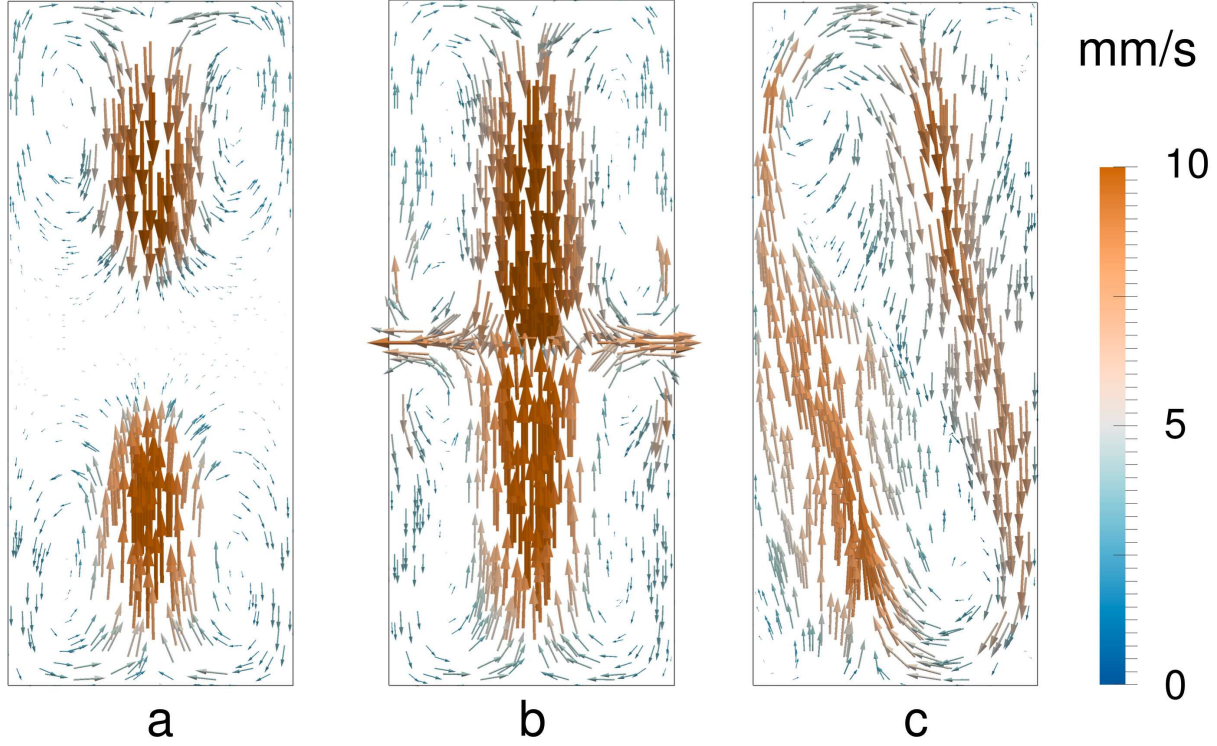


FIG. 11. Temporal development of the electro-vortex flow. The geometry consists of a cylindrical liquid metal column ( $D = 1$  m,  $H = 2.4$  m) with two current collectors ( $H_{cc} = 0.5$  m,  $\sigma_{cc}/\sigma = 5$ ) and an applied current corresponding to  $Ha = 100$ . The original  $m = 0$  mode (a: after 200 s) becomes unstable (b: after 400 s) and turns into a  $m = 1$  mode (c: after 2300 s).

the current is purely vertical and uniform only in the feeding line sufficiently far away from the current collectors. As the current enters the current collector, it spreads radially over the whole diameter (see the typical current structure in Fig. 10b for the upper and Fig. 10c for the lower current collector). Switching to the liquid metal column in Fig. 10d, we observe that the current is not completely homogeneous. In Fig. 10e we show the deviation of the Lorentz force from its uniform distribution in an infinite liquid metal column. The resulting force is no longer irrotational, as in the case of axially uniform base current considered before, and thus it cannot be balanced by the pressure gradient. This disbalance drives the so-called electro-vortex flow<sup>23</sup>.

In contrast to the TI, there is no threshold current for the onset of electro-vortex flows. Although electro-vortex flow starts as soon as the current is applied, some time is required for the flow to develop through the whole volume (Fig. 11a-b). As one would deduce from

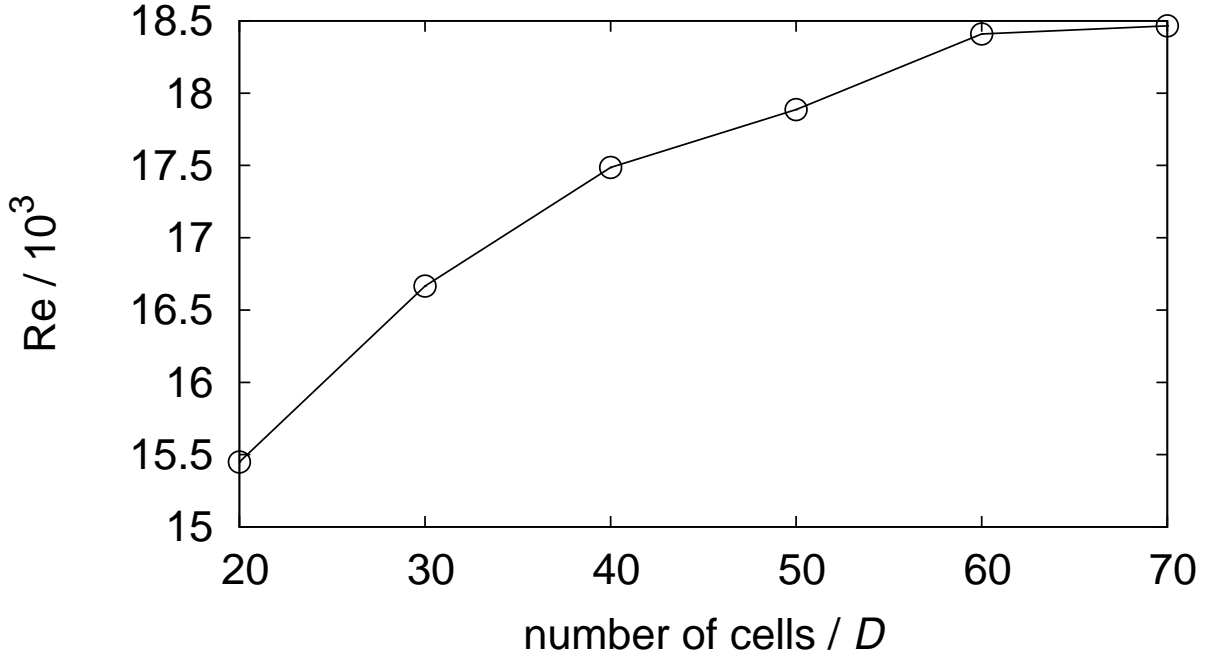


FIG. 12. Reynolds number associated with the electro-vortex flow in a cylindrical liquid metal column ( $D = 1$  m,  $H = 2.4$  m) with a current collector ( $H_{cc} = 0.5$  m,  $\sigma_{cc}/\sigma = 5$ ) and an applied current corresponding to  $Ha = 100$  for varying grid resolution.

the driving Lorentz forces (Fig. 10e), the initial flow structure is always axisymmetric, i.e.,  $m = 0$  mode. However, after some time, the electro-vortex flow often turns into a wind (see Fig. 11c). The time of transition depends not only on the applied current, but also on the aspect ratio and conductivity of current collectors and liquid metal column.

Similar to thermal convection, electro-vortex flows are often strongly time-dependent. Such simulation requires a much finer grid resolution than used for the TI by Weber et al.<sup>14</sup>. If we want to study the interaction of TI and electro-vortex flow, the latter should be rather weak to allow the TI to develop. Bearing these two things in mind, we choose the following simulation geometry: a relatively high liquid metal column ( $D = 1$  m,  $H = 2.4$  m) of aspect ratio 2.4 together with also high current collectors ( $H_{cc} > 0.5$  m). This configuration leaves enough “space” for the TI to develop, especially in the middle of the cylinder and ensures a stationary flow. In Fig. 12 we show the dependence of the Reynolds number on the grid resolution for this set-up. For our simulation we choose 25 purely cubic cells over the radius. The quadrature of the circle ensures a good azimuthal balance of the Lorentz forces (axial symmetry) (see also Fig. 10a). Flattening the current collectors below an aspect ratio of

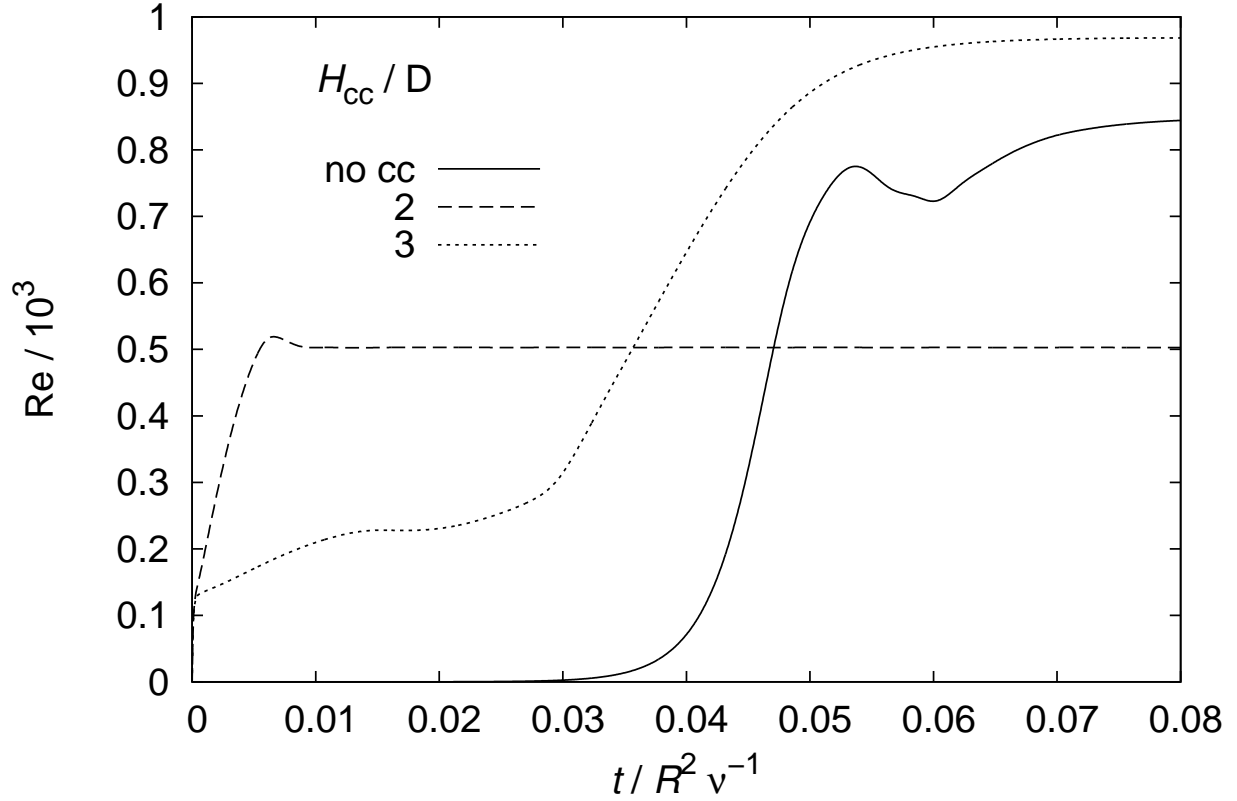


FIG. 13. Reynolds number in a cylindrical liquid metal column ( $D = 1$  m,  $H = 2.4$  m) for an applied current corresponding to  $Ha = 100$ . Simulation is carried out without current collector (straight line) and a current collector of aspect ratio 2 (dashed line) or 3 (dotted line) with an electric conductivity of  $\sigma_{cc}/\sigma = 5$ .

0.5 increases the Lorentz forces further and would definitely lead to an instationary electro-vortex flow.

Having clarified the geometry, grid resolution and initial fields, we will investigate now the interaction of electro-vortex flows with the TI. The TI usually growing exponentially needs some time to develop until it reaches saturation (see the black line in Fig. 13). We use this simulation of a liquid metal column of aspect ratio  $H/D = 2.4$  as reference and add current collectors of aspect ratio  $H_{cc}/D = 2$  (see the dashed line in Fig. 13). While the pure TI evolves very slowly (black line), the electro-vortex flow (dashed line) appears instantaneously at the start of the simulation. Nevertheless, electro-vortex flow, which initially starts at the current collectors, needs some time to spread over the whole volume.

This spreading makes the kinetic energy grow linearly until a certain saturation level is attained. Although this energy is lower than the saturation level of the TI, the latter does not develop here because the electro-vortex flow presumably disturbs the flow field in such a way so that to suppress the TI. In order to study TI and electro-vortex flow together, we increase the current collectors height to an aspect ratio of  $H_{cc}/D = 3$  which lowers radial currents and thus reduces the Lorentz force and the associated electro-vortex flow (see the dotted line in Fig. 13). The first initial rise of kinetic energy, which is the same as for short current collectors, is followed by a much slower linear “growth phase” of the electro-vortex flow. Of course, a weak flow needs more time to spread trough the whole volume. After the electro-vortex flow reaches its saturation level, the TI starts to develop and shortly an exponential growth of energy can be observed. As expected, the final saturation level lies slightly above the one of the simulation without current collectors – compare the straight and dotted line of Fig. 13. Obviously, the TI arises only under favourable conditions: long and good conducting current collectors, or possibly, also long liquid metal columns.

In order to study the influence of  $Ha$ , the aspect ratio and conductivity of the current collectors on the electro-vortex flows we will omit the TI in the following. Figure 14 shows the Reynolds number in dependence of the Hartmann number in a liquid metal column of aspect ratio  $H/D = 2.4$  with relatively flat current collectors. The relation is nearly linear. Compared to the TI, the magnitude of electro-vortex flow is relatively high also for low Hartmann numbers. In contrast to the TI, there is no critical current, i.e. already arbitrary small Hartmann numbers will induce a fluid flow. Note also that the relatively thick feeding line ( $D_{fl}/D = 0.5$ ) used here and the high aspect ratio of the liquid metal cylinder ( $H/D = 2.4$ ) may underestimate the electro-vortex flow taking place in a real liquid metal battery.

With a constant current ( $Ha = 100$ ) and the geometry as before, we alter the conductivity of the current collectors (see Fig. 15). Using perfectly conducting current collectors, the currents will homogenise already in the current collector. Thus, we expect no radial currents and very little Lorentz forces in the liquid metal. The curve in Fig. 15 will therefore approach asymptotically zero. Using a poor conductor for the current collector leads to more radial currents in the liquid. The increasing Lorentz forces will induce a larger fluid flow. Concerning liquid metal batteries, Fig. 15 reveals two things. Firstly, the current collector should have a good conductivity in order to minimise material requirements. Secondly, the

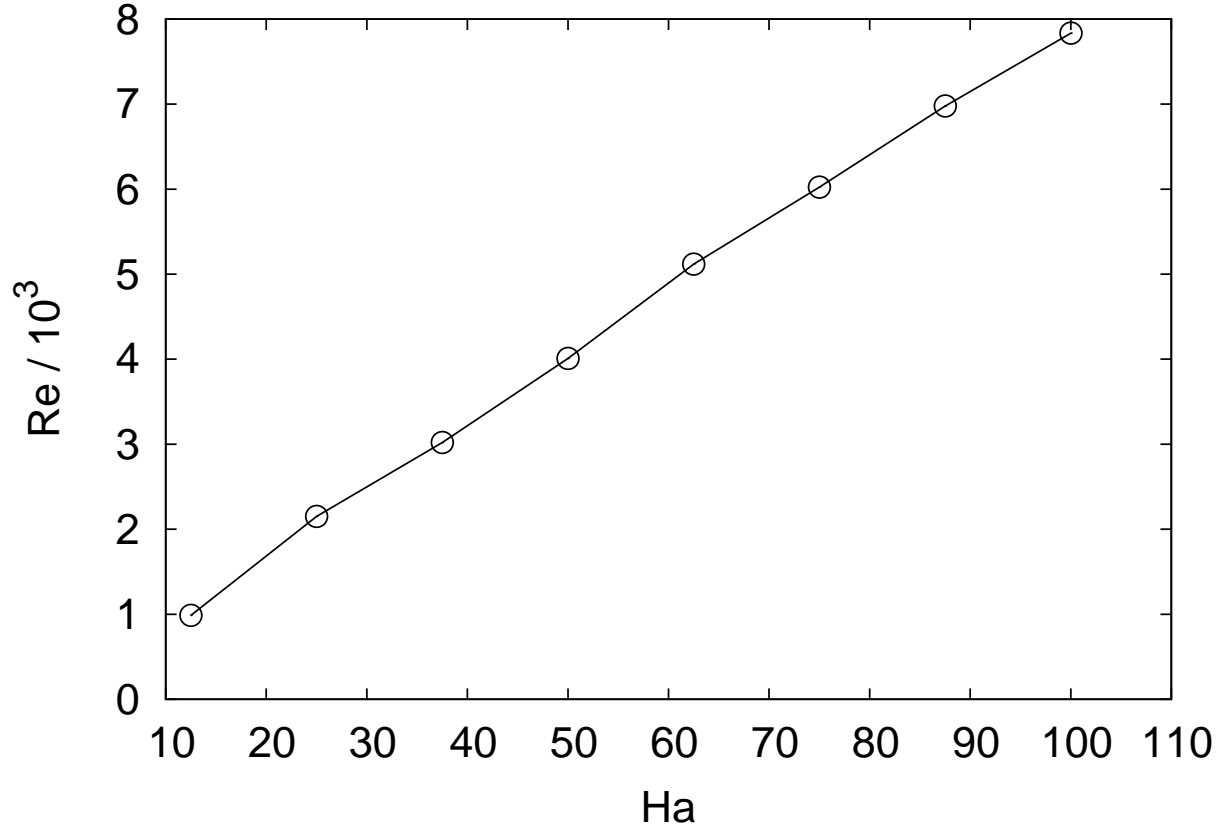


FIG. 14. Reynolds number of the electro-vortex flow against the Hartmann number. The geometry consists of a cylindrical liquid metal column ( $D = 1$  m,  $H = 2.4$  m) with two current collectors ( $H_{cc} = 0.5$  m,  $\sigma_{cc}/\sigma = 5$ ).

conductivity has to be considered relative to that of the liquid metal. The biggest changes are expected in the vicinity of  $\sigma_{cc}/\sigma = 1$ .

Assuming a fixed (dis-)charging current, the most important parameter determining the flow velocity is the aspect ratio of current collectors (Fig. 16). In the collectors of infinite height, the current will redistribute uniformly producing no electro-vortex flow. With a decrease of the aspect ratio, the kinetic energy of the liquid metal increases exponentially. Especially going below an aspect ratio of  $H_{cc}/D = 1$  produces a considerable flow in the fluid. The effect of the aspect ratio of current collectors is important for flat collectors but marginal for extended ones.

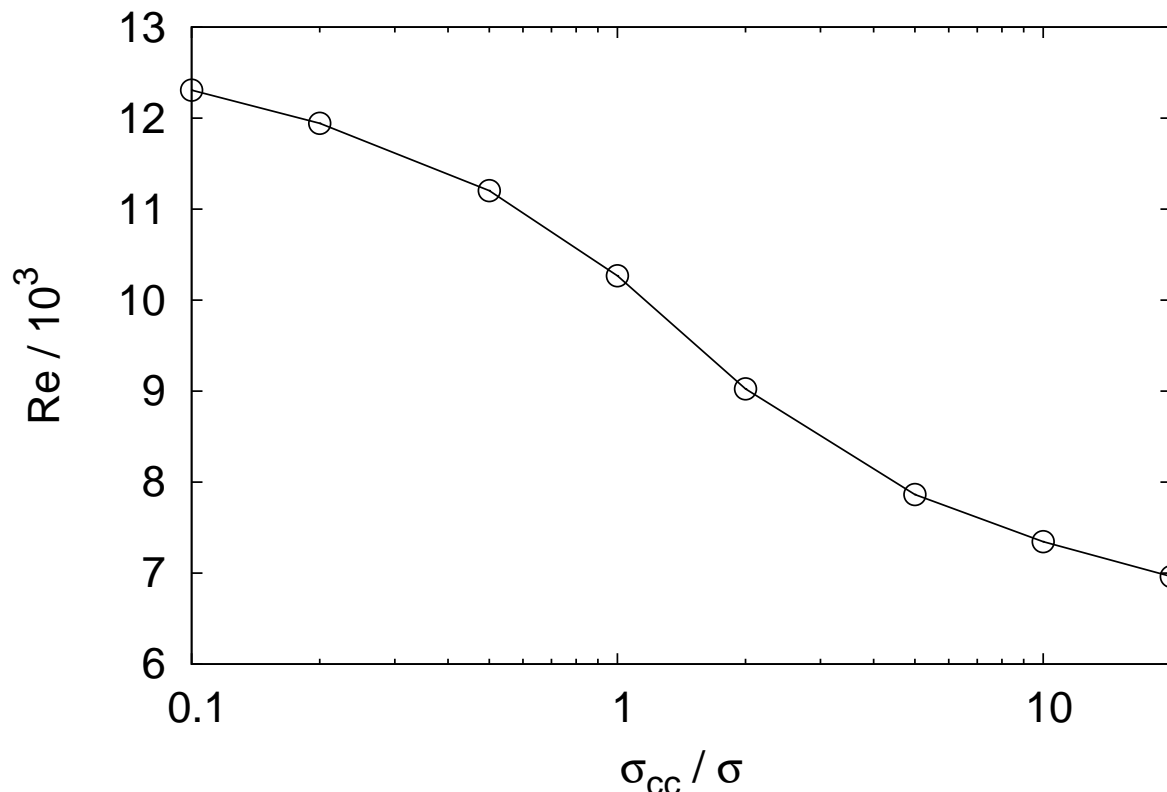


FIG. 15. Reynolds number of the electro-vortex flow ( $Ha = 100$ ) in a cylindrical liquid metal column ( $D = 1$  m,  $H = 2.4$  m) with two current collectors of aspect ratio  $H_{cc}/D = 0.5$ . Only the electric conductivity of the current collectors is changed.

## V. CONCLUSIONS AND PROSPECTS

The first objective of this paper was to estimate the effects of the current distribution in the solid current collectors on properties of the Tayler instability in liquid metals. For this purpose, we have enhanced the integro-differential equation approach, as developed by Weber et al.<sup>14</sup>, by a detailed computation of the electric potential and the current distribution in the current collectors. This was accomplished by solving the Laplace equation in the solid region and by matching this solution in an iterative way to the solution of the Poisson equation in the liquid metal.

Our main conclusion is that the consideration of realistic current collectors has certain effects on the TI which make them essential for a realistic simulation. However, in a real fluid flow, thermal convection and electro-vortex flow will have a much larger influence on

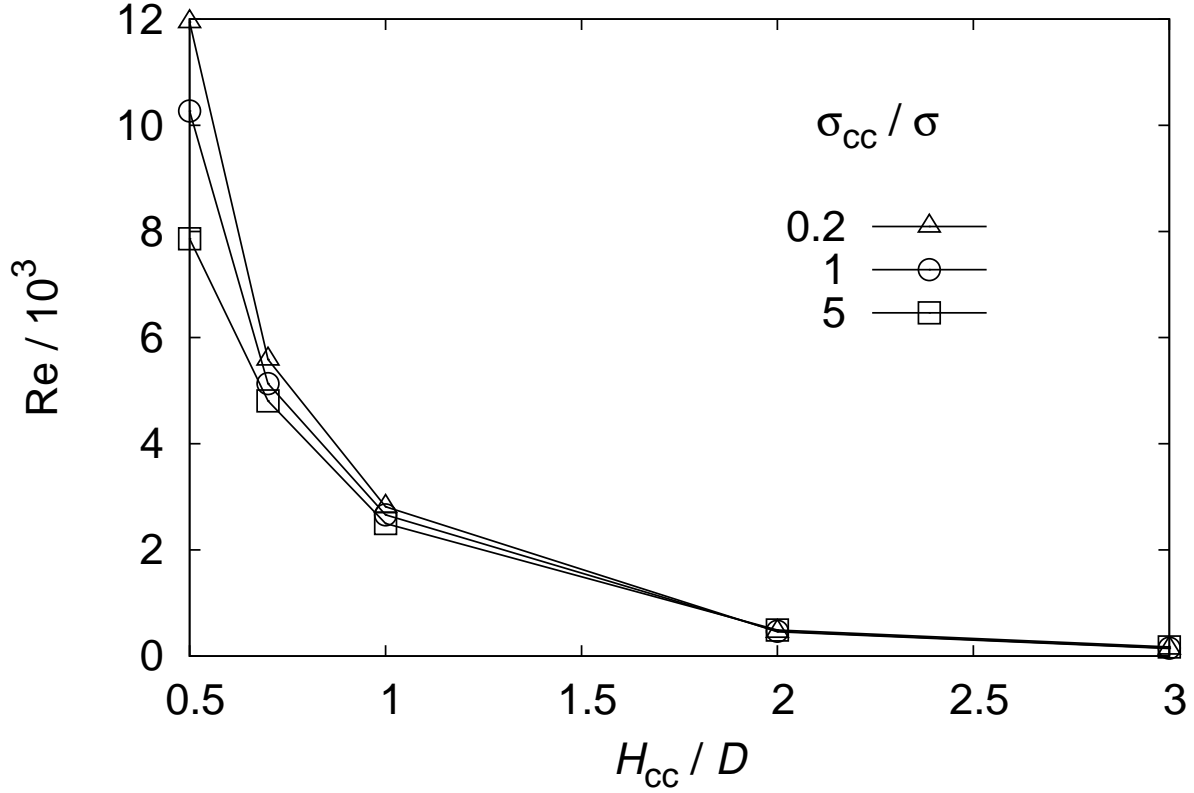


FIG. 16. Reynolds number in a cylindrical liquid metal column ( $D = 1$  m,  $H = 2.4$  m) for different current collector aspect ratios and  $Ha = 100$ .

the TI. Therefore, it seems somehow justified to work with simplified boundary conditions such as  $\varphi = const$  for a first estimate, bearing in mind the underestimation of the growth rate and flow velocity.

Secondly, we have included the feeding lines into our simulation by solving a coupled Laplace equation for the static potential in the liquid metal and current collectors. Flowing from the thin wire into the wide current collector, the electric current acquires radial components, resulting in electro-vortex flow. Depending on the geometry of battery, current collectors and their conductivities, these flows can be quite strong and may impede the development of the TI.

In LMBs, strong electro-vortex flows have to be avoided in order to maintain the integrity of the thin electrolyte layer. This may be achieved by an appropriate design of the current collectors. Of course, a solid metal cylinder with an aspect ratio  $H/D = 1$  will get heavy

and costly, but a careful distribution of the charging current by several (thin) wires may solve the problem. A more detailed design will require further studies under the cost aspect.

While a strong mixing of the LMB must be avoided, a slight fluid flow in the lower compartment can be advantageous. Reaction products, as, e.g. intermetallic phases which would limit the mass transfer at the interface may be spread in the alloy by a slow fluid flow. Again, this can be achieved by an appropriate geometry of the positive current collector. Here, not only aspect ratio and conductivity will be of interest, but also surface shaping, coating, etc. are possible options. Further numerical and experimental studies will be required.

Apart from studying the TI and electro-vortex flow, the methodology developed here can be useful when it comes to a realistic simulation of the interaction of the TI in the bulk of the fluid with various types of interfacial instabilities between the layers of a LMB. Work on this problem is currently under way.

## ACKNOWLEDGEMENTS

This work was supported by Helmholtz-Gemeinschaft Deutscher Forschungszentren (HGF) in frame of the “Initiative für mobile und stationäre Energiespeichersysteme”, and in frame of the Helmholtz Alliance LIMTECH, as well as by Deutsche Forschungsgemeinschaft in frame of the SPP 1488 (PlanetMag).

## REFERENCES

- <sup>1</sup>H. Goedbloed and S. Poedts, *Principles of Magnetohydrodynamics* (Cambridge University Press, 2004).
- <sup>2</sup>G. Rüdiger, M. Schultz, and M. Gellert, “The Tayler instability of toroidal magnetic fields in a columnar gallium experiment,” *Astron. Nachr.* **10**, 1 – 7 (2011).
- <sup>3</sup>M. Seilmayer, F. Stefani, T. Gundrum, T. Weier, G. Gerbeth, M. Gellert, and G. Rüdiger, “Experimental evidence for a transient Tayler instability in a cylindrical liquid-metal column,” *Phys. Rev. Lett.* **108** (2012).
- <sup>4</sup>H. C. Spruit, “Dynamo action by differential rotation in a stably stratified stellar interior,” *Astron. Astrophys.* **381**, 923 – 932 (2002).



- <sup>5</sup>M. P. L. Suijs, N. Langer, A.-J. Poelarends, S.-C. Yoon, A. Heger, and F. Herwig, “White dwarf spins from low mass stellar evolution models,” *Astron. Astrophys.* **481**, L87 – L90 (2008).
- <sup>6</sup>H. Kim, D. A. Boysen, J. M. Newhouse, B. L. Spatocco, B. Chung, P. J. Burke, D. J. Bradwell, K. Jiang, A. A. Tomaszowska, K. Wang, W. Wei, L. A. Ortiz, S. A. Barriga, S. M. Poizeau, and D. R. Sadoway, “Liquid metal batteries: Past, present, and future,” *Chem. Rev.* **113**, 2075 – 2099 (2013).
- <sup>7</sup>N. Weber, V. Galindo, F. Stefani, and T. Weier, “Current-driven flow instabilities in large-scale liquid metal batteries, and how to tame them,” *J. Power Sources* **265**, 166 – 173 (2014).
- <sup>8</sup>F. Stefani, T. Weier, T. Gundrum, and G. Gerbeth, “How to circumvent the size limitation of liquid metal batteries due to the Tayler instability,” *Energ. Convers. Manage.* **52**, 2982 – 2986 (2011).
- <sup>9</sup>L. A. Herédy, M. L. Iverson, G. D. Ulrich, and H. L. Recht, “Development of a thermally regenerative sodium-mercury galvanic system part I electrochemical and chemical behavior of sodium-mercury galvanic cells,” in<sup>24</sup>, pp. 30 – 42.
- <sup>10</sup>B. Agruss and H. R. Karas, “The thermally regenerative liquid metal concentration cell,” in *Regenerative EMF cells*, Advances in Chemistry, Vol. 64, edited by R. F. Gold (American Chemical Society, Washington, D.C., 1967) pp. 62 – 81.
- <sup>11</sup>M. S. Foster, “Laboratory studies of intermetallic cells,” in<sup>24</sup>, pp. 136 – 148.
- <sup>12</sup>E. J. Cairns, C. E. Crouthamel, A. K. Fischer, M. S. Foster, J. C. Hesson, C. E. Johnson, H. Shimotake, and A. D. Tevebaugh, *Galvanic Cells with Fused-Salt Electrolytes*, ANL-7316 (Argonne National Laboratory, 1967).
- <sup>13</sup>D. H. Kelley and D. R. Sadoway, “Mixing in a liquid metal electrode,” *Physics of Fluids* **26** (2014).
- <sup>14</sup>N. Weber, V. Galindo, F. Stefani, T. Weier, and T. Wondrak, “Numerical simulation of the Tayler instability in liquid metals,” *New J. Phys.* **15** (2013).
- <sup>15</sup>F. Stefani, G. Gerbeth, and A. Gailitis, “Velocity profile optimization for the Riga dynamo experiment,” in *Transfer Phenomena in Magnetohydrodynamics and Electrocinducting flows*, edited by A. Alemany, P. Marty, and J. P. Thibault (Kluwer Dordrecht, 1999) pp. 31 – 44.

- <sup>16</sup>J.-L. Guermond, R. Laguerre, J. L  orat, and C. Nore, “An interior penalty Galerkin method for the MHD equations in heterogeneous domains,” *J. Comput. Phys.* **221**, 349 – 369 (2007).
- <sup>17</sup>F. Stefani, G. Gerbeth, and K.-H. R  dler, “Steady dynamos in finite domains: an integral equation approach,” *Astron. Nachr.* **321**, 65 – 73 (2000).
- <sup>18</sup>A. Iskakov, S. Descombes, and E. Dormy, “An integro - differential formulation for magnetic induction in bounded domains: boundary element - finite volume method,” *J. Comput. Phys.* **197**, 540 – 554 (2004).
- <sup>19</sup>A. Giesecke, F. Stefani, and G. Gerbeth, “Kinematic simulations of dynamo action with a hybrid boundary-element/finite-volume method,” *Magnetohydrodynamics* **44**, 237 – 252 (2008).
- <sup>20</sup>A. J. Meir, P. G. Schmidt, S. I. Bakhtiyarov, and R. A. Overfelt, “Numerical simulation of steady liquid – metal flow in the presence of a static magnetic field,” *J. Appl. Mech.* **71**, 786 – 795 (2004).
- <sup>21</sup>P. A. Davidson, *An Introduction to Magnetohydrodynamics* (Cambridge University Press, 2001).
- <sup>22</sup>A. Bonanno, A. Brandenburg, F. Del Sordo, and D. Mitra, “Breakdown of chiral symmetry during saturation of the Tayler instability,” *Phys. Rev. E* **86** (2012).
- <sup>23</sup>V. Bojarevi  s, Y. Freibergs, E. I. Shilova, and E. V. Shcherbinin, *Electrically induced vortical flows*, edited by R. J. Moreau and G. Oravas (Kluwer Academic Publishers, 1989).
- <sup>24</sup>C. Crouthamel and H. Recht, eds., *Regenerative EMF Cells*, Vol. 64 (American Chemical Society, 1967).